Sensitivity of Horizontal Ribbon Growth to Solidification Kinetics

Nojan Bagheri-Sadeghi[a], Victor A. Fabiyi[b], Brian T. Helenbrook[a,*], Eunsu Paek[b]

[a] *Department of Mechanical & Aerospace Engineering, Clarkson University, Potsdam, NY 13699-5725, United States*
[b] *Department of Chemical and Biomolecular Engineering Engineering, Clarkson University, Potsdam, NY 13699, United States*

Abstract

Simulations of horizontal ribbon growth of silicon using a high-order finite element method were used to assess the sensitivity of results to the coefficients used in the solidification kinetics model. The position of the leading edge of the silicon sheet showed little sensitivity to the kinetic coefficient of roughened growth or step propagation. However, there was a significant difference in the leading edge position and maximum pull speed predictions between three correlations of two-dimensional nucleation of silicon proposed in the literature. The deviation between the results using the three correlations increased with increasing pull speed. The significant sensitivity of results to two-dimensional nucleation coefficient indicates the importance of accurate modeling of the two-dimensional nucleation for horizontal ribbon growth of silicon and the possibility of using HRG experiments to help improve models of two-dimensional nucleation.

Keywords: A1 Computer simulation, A1 Growth models, A1 Interfaces, A1 Kinetics, A2 Growth from melt, B2 Semiconducting silicon

*Corresponding author
Email address: bhelenbr@clarkson.edu (Brian T. Helenbrook)

1. Introduction

Experimental studies of horizontal ribbon growth (HRG) of silicon have shown formation of a {111} facet near the leading edge of the sheet [1–3]. The formation of this facet is associated with the kinetic mechanisms of two-dimensional (2D) nucleation and step propagation along the facet [4–6]. 2D nucleation has proven difficult to model and there is a lot of uncertainty in predictions of 2D nucleation. For example, Edwards [7], Voronkov [8], and Abe [9] all estimated the supercooling associated with 2D nucleation in Czochralski growth and the predictions ranged from 1.5 to 9 K. There are also several different 2D nucleation kinetic models proposed in the literature [5, 10, 11]. These models vary significantly in their dependence on the supercooling temperature and are used for simulation of faceted crystals grown from melt using various growth techniques [1, 5, 12–19].

To simulate HRG, Helenbrook et al. [1] used the solidification kinetics model proposed by Weinstein and Brandon [5], which includes terms that model 2D nucleation and step propagation as well as roughened growth. They were able to predict the existence of a facet near the triple phase junction(TPJ), where the cooling helium jet, liquid and solid silicon meet. Helenbrook et al. [1] also showed a maximum pull speed limit dictated by solidification kinetics as a result of a turning point in the response of leading edge position to pull speed. Beyond the maximum pull speed steady solutions cease to exist. This limit is a result of kinetics; HRG models without kinetics concluded that there was no upper bound for pull speed [20–23] or that it was determined by other effects [24, 25].

The purpose of this paper is to assess the sensitivity of HRG simulation results to the values of kinetic coefficients of roughened growth, step propagation, and three different correlations proposed for 2D nucleation of silicon [5, 10, 11, 26, 27]. The main point of comparison will be the position of the leading edge of growth as a function of pull speed. This has been measured experimentally, so can help determine which models better predict reality. A further goal of the paper is to assess the dependence of the predicted maximum

pull speed on the kinetic parameters. Accurately predicting this pull speed is critical to assessing the commercial viability of HRG.

2. Methods

The HRG experiment and corresponding numerical model are described in [1, 2, 28]. Here, we just give a brief overview, mainly focusing on the kinetics model and the parameters therein. The experiment detailed in [1, 2] had sections for replenishment, growth, thickness control, separation and removal of silicon sheets consecutively. As in [1, 28] only the growth section of the experiment was modeled.

A schematic of the growth section and an adapted mesh comprised of a liquid region Ω_l and a solid region Ω_s are shown in Fig. 1a-b. The depth of the domain is $d = 13$ mm. The cooling needed for solidification was provided by a helium jet impinging on the top of the domain, which was modeled as a heat flux boundary condition on the top surface. This heat flux was obtained from a curve fit to the results of helium jet impingement simulations as a combination of two Gaussian distributions and a constant (see [1]).

The convection-diffusion equation was solved for the temperature, T, in the solid. The velocity of the solid silicon only had a horizontal component, $u_{s,1}$, equal to the constant pull speed. For liquid, in addition to the convection-diffusion equation, continuity and Navier-Stokes equations of an incompressible Newtonian fluid were solved.

At the solidification interface, conservation of mass and energy were imposed. The solidification kinetics was based on the model in [5]

$$\Delta T = K(\Delta T, \theta_m) V_g \tag{1}$$

where the supercooling temperature $\Delta T = T_m - T$, T is the supercooled interface temperature and $T_m = 1685$ K is the equilibrium melting temperature of silicon, and V_g is the solidification growth velocity. The kinetic coefficient, $K(\Delta T, \theta_m)$ is a function of ΔT, and the misalignment angle, θ_m, from the $\{111\}$ facet

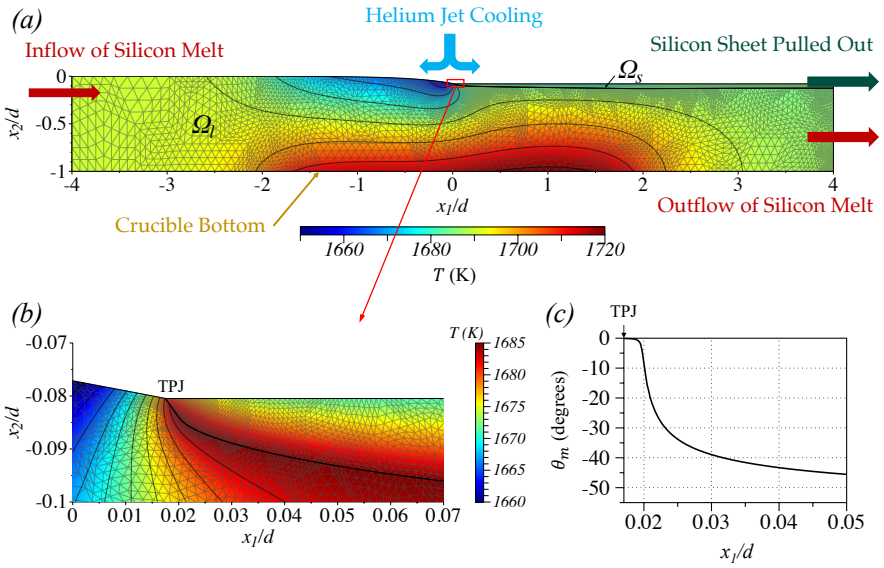

Figure 1: Steady state solution for case 1 with correlation 2 for K_{2DN} at $u_{s,1} = 3.8$ mm/s (a) The schematic, sample mesh and the temperature contours at 10 K intervals (b) Zoomed-in view of temperature contours and mesh near the TPJ with temperature contours at 2.5 K intervals (c) The misalignment angle of the solid-liquid interface from {111} facet as a function of position

direction. The {111} plane is about 55° from the horizontal axis assuming that the growth initiated with [$\bar{1}$00] and [011] directions pointing upward and aligned with the growth direction respectively.

The interface was assumed to be dislocation-free [29] and the overall kinetic coefficient was defined as

$$\begin{cases} K = K_{2DN}, & \text{TPJ} \\ K = \left(K_{rough}^4 + K_{step}^4\right)^{1/4}, & \text{elsewhere} \end{cases} \tag{2}$$

where the kinetic coefficient of two-dimensional nucleation (2DN), which determines the supercooling occurring at the TPJ, is given by:

$$K_{2DN} = B^{-1} e^{\frac{A}{\Delta T}} \Delta T^n$$

Three sets of values for A, B and n from literature were used as given in Table 1.

Table 1: Values of constants A, B and n in 2D nucleation correlation

Correlation	A (K)	B	n	Reference
1	46.67	2.22×10^{-1} m/(s $\cdot$ K$^{2/3}$)	$\frac{1}{3}$	[10, 26, 27]
2	140	1.5×10^{10} m/(s $\cdot$ K)	0	[5]
3	14.64	3.42×10^{-1} m/(s $\cdot$ K$^{2/3}$)	$\frac{1}{3}$	[11]

Correlation 1 is based on a nucleation rate determined from Monte Carlo simulations in [10], with the corrected correlation given in [27], and the polynuclear 2D nucleation expression of [30] with simplifications given in [26]. Correlation 2 is from [5] which simplifies the original analytically derived equation of [8, 31, 32] by approximating $n = 5/6$ in the original equation with $n = 1$. Correlation 3 is obtained from a 2D nucleation rate estimated from molecular dynamics simulations and the the polynuclear 2D nucleation expression of [30].

The kinetic coefficient of the step propagation mechanism K_{step} was given by:

$$K_{step} = \frac{K_{SN}}{|\sin(\theta_m)| + \epsilon_{step}}$$

where $K_{SN} = 1/0.63$ K s/m [8] and the value of ϵ_{step} was set to machine precision to avoid dividing by zero. At large misalignment angles the kinetic coefficient of roughened growth, $K_{rough} = 1/0.122$ K s/m [33], becomes dominant.

Compared to the formulation in [1], there are a few minor changes. As described in [28], a growth angle at the TPJ was added to the model. For simplicity Marangoni and buoyancy effects (investigated in [28]) were not included. All remaining boundary conditions were set the same as [28]. For the thermal boundary condition on the top of the domain, which models the helium jet, the three heat flux cases 1 to 3 in Ref. [1] were simulated corresponding to three different experiments. The peak convective heat flux of each case is given in Table 2.

A high-order finite element method (hp-FEM) was used with fourth-degree basis functions, and an arbitrary-Lagrangian-Eulerian (ALE) moving mesh with

Table 2: The peak heat flux of helium jet heat fluxes studied corresponding to three experimental cases in [1]

Case	q_{peak} (MW/m^2)
1	2.53
2	3.50
3	3.75

mesh adaptation was used to track the solid-liquid interface [34]. This method provides fifth order spatial accuracy if the solution in the solid and liquid domain is smooth.

3. Results and Discussion

The steady state contours of temperature are shown in Fig 1a-b at $u_{s,1} = 3.8$ mm/s for case 1 using correlation 2 for K_{2DN}. This was the greatest pull speed for which a solution was obtained and corresponds to the turning point behavior discussed in [1]. The TPJ is the coldest point on the interface, and this is where 2D nucleation is assumed to occur. The step propagation mechanism dominates near the TPJ where a vicinal surface with a small misalignment angle is formed as shown in Fig. 1c. After the small facet, there is sharp increase in the misalignment angle and the solidification kinetics becomes dominated by roughened growth.

3.1. Grid Validation

Before examining the kinetic coefficients, a grid convergence study was performed to evaluate the sensitivity of the TPJ position to grid resolution for case 1 with correlation 2 for K_{2DN}. The target truncation error used for mesh adaptation was reduced by a factor of 10 for each finer mesh. At $u_{s,1} = 3.8$ mm/s, corresponding to the turning point, the position of TPJ was at x_1/d of 0.01751, 0.01736, and 0.01704 for the coarse, medium and fine meshes with about 4000, 8700 and 20000 degrees of freedom respectively. This is about 1.9% difference

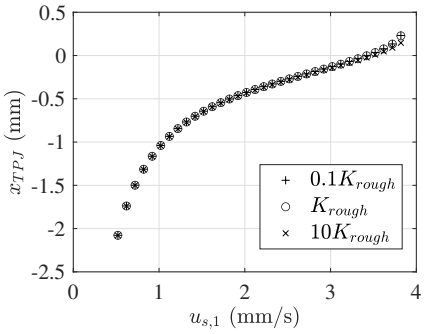

Figure 2: The sensitivity of position of TPJ to the kinetic coefficient of rough growth, K_{rough} for case 1 with correlation 2 for K_{2DN}

between the medium and fine grids. At lower pull speed the solution was even less sensitive to the grid resolution. This is not significant relative to the sensitivities to kinetics parameters discussed below. For the cases discussed below, the target error was set equal to that of the medium mesh.

3.2. K_{rough}

Fig. 2 shows the sensitivity of the position of TPJ to the kinetic coefficient for roughened growth, K_{rough} when it was decreased or increased by a factor of 10 with correlation 2 for K_{2DN}. There is only a small deviation in x_{TPJ} at greater pull speeds for the case with the value of K_{rough} increased by a factor of 10. The shape of the interface was not significantly changed as well by these changes in K_{rough}. When using the other two correlations for 2D nucleation they were similarly insensitive to K_{rough}. Thus, uncertainties in the value of K_{rough} should not significantly change the solution.

3.3. K_{step}

The sensitivity of x_{TPJ} to the kinetic coefficient of the step propagation mechanism, K_{step} is illustrated in Fig. 3 for case 1 with correlation 2. Reducing the coefficient by an order of magnitude barely changes the x_{TPJ} as shown in Fig. 3. However, using a smaller K_{SN} made it more difficult to obtian converged

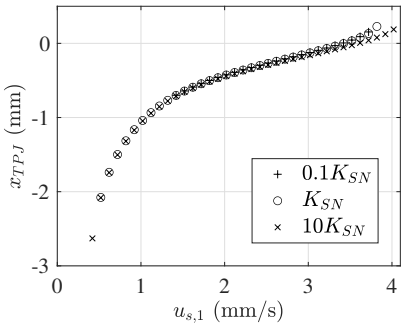

Figure 3: The sensitivity of position of TPJ to the kinetic coefficient of step propagation mechanism, $K_{step} = \frac{K_{SN}}{|\sin\theta_m|}$ for case 1 with correlation 2 for K_{2DN}

solutions, especially at lower pull speeds. The main deviation of the case with 10 times larger K_{SN} is seen at higher pull speeds where the x_{TPJ} is predicted further upstream. This caused an increased pull speed at the turning point.

The sensitivity of the solution to K_{step} at higher pull speeds was slightly dependent on the correlation used for K_{2DN}. The correlations 1 and 3 were respectively least and most sensitive to variations in K_{step}. For instance, an increase in K_{SN} by a factor 10 for case 1, resulted in the maximum pull speed of correlations 1 to 3 increase by about 4%, 5% and 15 % respectively. The results of correlation 2 are shown here as they showed an intermediate sensitivity to K_{step}.

Changing the value of K_{SN} changed the length or existence of the facet as shown in Fig. 4, which shows the misalignment angle as a function of x_1/d. The facet is the region where the misalignment angle is near 0. At the decreased value of K_{SN} the length of the facet slightly increased followed by a sharper increase in misalignment angle at the end of the facet. At the increased value of K_{SN} the facet basically disappeared. We note that although increasing K_{SN} makes this problem easier to converge, making K_{SN} artificially large as we did in [28] can significantly change the behavior because the facet disappears.

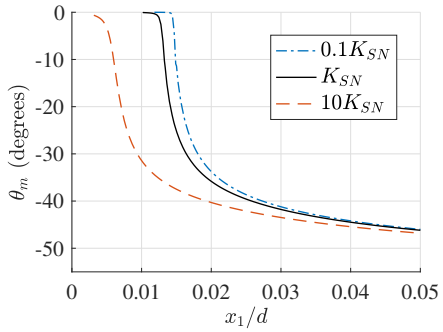

Figure 4: The sensitivity of the misalignment angle, characterizing the solidification interface shape, to the step propagation mechanism, $K_{step} = \frac{K_{SN}}{|\sin\theta_m|}$ for case 1 with correlation 2 for K_{2DN}

3.4. K_{2DN}

Fig. 5 shows the sensitivity of x_{TPJ} to the kinetic coefficient of 2D nucleation. Three different correlations with constants given in Table 1 were used. Fig. 5a-c correspond to cases 1 to 3 from Ref. [1] with three different values of maximum helium jet cooling as tabulated in Table 2. There is a significant difference between predictions of x_{TPJ} among three correlations. The 2D nucleation determines the maximum supercooling at the TPJ and therefore can significantly change the solution near the TPJ. For all three cases correlations 1 and 3 predicted the lowest and highest pull speeds for the turning point.

Fig. 5 also shows experimental data from [1] with error bars. The error bars are based on the accuracy of optically determining the position of the solidification leading edge. There are also errors in determining the experimental operating conditions such as heat fluxes, pull speeds, and gas flow rates which are propagated to the model predictions. In addition, the current model does not include Marangoni, buoyancy, or gas flow effects on the heat transfer. Our previous study showed that with the Marangoni effects are included at a given pull speed the TPJ moves further downstream by about 0.1- 0.2 mm at a given pull speed, and the maximum pull speed attainable reduces (see Fig. 13 in [1]). In our recent work [28], we also showed that Marangoni and buoyancy effects

lead to flow instabilities that result in variations in triple junction position on the order of a tenth of millimeter. In spite of these differences, all three correlations' predictions are close to the experimental data because the sensitivity is less at low pull speeds. The deviations among the correlations in Fig. 5 increase at higher pull speeds.

For all three correlations shown in Fig. 5 at a given pull speed, the TPJ position moved further upstream going from case 1 to 2 to 3. The cooling profiles were characterized by the peak cooling flux, q_{peak} as given in Table 2 and a parameter in the Gaussian cooling profile corresponding to the width of the jet (see [1, 28]). The peak heat flux increased by 38% and 7% from case 1 to 2 and from case 2 to 3 respectively. Moreover, the parameter corresponding to the width of the jet decreased by about 10% each time going from case 1 to 3. The movement of x_{TPJ} further upstream at a given pull speed and the increase in the maximum pull speed from case 1 to 3 for all three correlations mainly is a result of the increase in q_{peak}. Between cases 2 and 3 the effect of a sharper temperature gradient in case 3 is reflected in greater disparity between the different correlations at lower pull speeds. This greater sensitivity of case 3 makes it a better choice than other two configurations for studying 2D nucleation.

Due to simplifying assumptions in the model and the limited experimental data no conclusions can be drawn about the accuracy of these 2D nucleation correlations. However, the sensitivity of the results to these 2D nucleation correlations where there is a factor of 2 difference between the pull speed of the turning point, shows the importance of an accurate correlation for 2D nucleation. This high sensitivity makes HRG experiments potentially useful for investigating 2D nucleation models if careful experiments can be done at higher pull speeds.

The size of the facet, and the amount of supercooling were sensitive to the kinetic coefficient of 2D nucleation. Fig. 6 shows that the facet size increased for correlations 1 to 3 respectively. At 2.5 mm/s, which is near the turning point for case 1, the facet lengths for correlations 1 to 3 shown in Fig. 6 are about

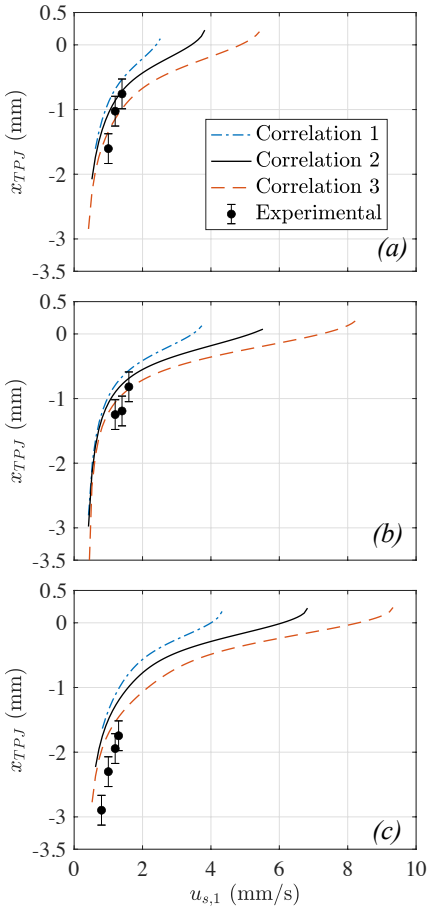

Figure 5: The sensitivity of the position of x_{TPJ} to the correlation for kinetic coefficient of 2D nucleation and experimental data from [1] for (a) case 1 (b) case 2 (c) case 3

0.066, 0.036, and 0.017 mm, which is about a factor of 4 change in facet length.

Figure 7 shows supercooling in terms of the growth rate calculated at the triple junction. Additionally, experimental data of supercooling versus growth rate from Czochralski growth [7–9] and float-zone growth [35] are also shown. An average growth rate is used for [9, 35] since only a range of growth rates are given for the estimated supercooling. The supercooling values in these papers are roughly determined based on an estimated temperature gradient near the

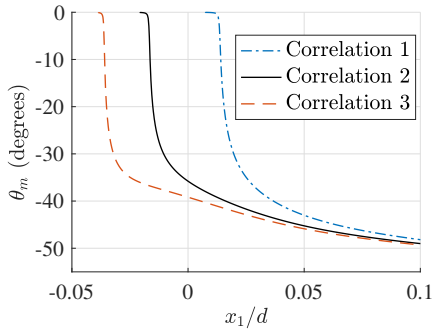

Figure 6: The sensitivity of the misalignment angle, characterizing the solidification interface shape, to the K_{2DN} correlation for case 1 at $u_{s,1} = 2.5$ mm/s

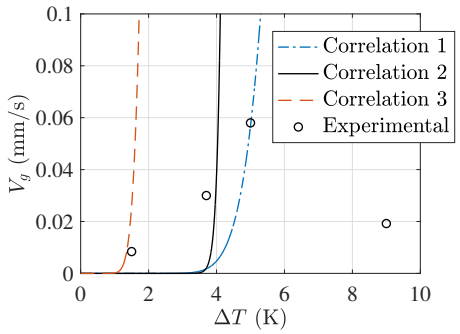

Figure 7: The growth velocity as a function of supercooling for three different correlations of 2D nucleations. The experimental data are from Refs. [7–9, 35]

TPJ with the assumption that the temperature of the non-faceted portion of the interface is the equilibrium melting temperature. The figure shows that correlations 1 to 3 respectively predicted the greatest to smallest supercooling at the TPJ. Prediction of correlation 1 is close to experimental data from [35], 2 is close to [35], and 3 is close to [7]. The scatter in the experimental data illustrates the need for more accurate experiments.

4. Conclusions

The sensitivity of numerical simulations of horizontal ribbon growth to the modeling of 2D nucleation, step propagation and roughened growth was studied. The results showed almost no sensitivity to the value of kinetic coefficient of roughened growth and a small sensitivity to the kinetic coefficient of step propagation at higher pull speeds. The main sensitivity was to the 2D nucleation coefficients. This affected the position of the TPJ as a function of pull speed, the maximum pull speed, the size of the leading edge facet, and the amount of supercooling. Unfortunately the experiments were not precise enough to determine which correlation was more physically accurate, but these results do indicate that modeling 2D nucleation accurately is essential for accurately predicting the behavior of HRG.

Acknowledgments

This material is based upon work supported by the National Science Foundation under Grant No. 1762802.

References

[1] B. T. Helenbrook, P. Kellerman, F. Carlson, N. Desai, D. Sun, Experimental and numerical investigation of the horizontal ribbon growth process, Journal of Crystal Growth 453 (2016) 163–172. doi:10.1016/j.jcrysgro.2016.08.034.

[2] P. Kellerman, B. Kernan, B. T. Helenbrook, D. Sun, F. Sinclair, F. Carlson, Floating silicon method single crystal ribbon – observations and proposed limit cycle theory, Journal of Crystal Growth 451 (2016) 174–180. doi:10.1016/j.jcrysgro.2016.07.012.

[3] P. Daggolu, J. Appel, P. Kellerman, N. Stoddard, Pulling thin single crystal silicon wafers from a melt: The new leading-edge solar substrate, Journal

of Crystal Growth 584 (2022) 126561. doi:10.1016/j.jcrysgro.2022.126561.

[4] A. A. Chernov, Growth mechanisms, in: Modern Crystallography III: Crystal Growth, Springer Berlin Heidelberg, 1984, pp. 104–158. doi:https://doi.org/10.1007/978-3-642-81835-6_3.

[5] O. Weinstein, S. Brandon, Dynamics of partially faceted melt/crystal interfaces I: computational approach and single step–source calculations, Journal of Crystal Growth 268 (1) (2004) 299–319. doi:10.1016/j.jcrysgro.2004.04.108.

[6] V. Voronkov, B. Dai, M. Kulkarni, 3.03 - fundamentals and engineering of the Czochralski growth of semiconductor silicon crystals, in: P. Bhattacharya, R. Fornari, H. Kamimura (Eds.), Comprehensive Semiconductor Science and Technology, Elsevier, Amsterdam, 2011, pp. 81–169. doi:https://doi.org/10.1016/B978-0-44-453153-7.00089-4.

[7] W. D. Edwards, Liquid–solid interface shape observed in silicon crystals grown by the Czochralski method, Canadian Journal of Physics 38 (3) (1960) 439–443. doi:https://doi.org/10.1139/p60-044.

[8] V. V. Voronkov, Supercooling at the face developing on a rounded crystallization front, Soviet Physics – Crystallography 17 (5) (1973) 807–813.

[9] T. Abe, The growth of Si single crystals from the melt and impurity incorporation mechanisms, Journal of Crystal Growth 24-25 (1974) 463–467. doi:https://doi.org/10.1016/0022-0248(74)90358-3.

[10] K. M. Beatty, K. A. Jackson, Monte carlo modeling of silicon crystal growth, Journal of Crystal Growth 211 (1) (2000) 13–17. doi:https://doi.org/10.1016/S0022-0248(99)00836-2.

[11] V. A. Fabiyi, T. Richmond, B. T. Helenbrook, E. Paek, Molecular dynamics determination of two-dimensional nucleation kinetic coefficient for modeling

the faceted growth of Si (111) from an undercooled melt, Journal of Crystal Growth 592 (2022) 126736. doi:https://doi.org/10.1016/j.jcrysgro.2022.126736.

[12] O. Weinstein, S. Brandon, Dynamics of partially faceted melt/crystal interfaces II: multiple step–source calculations, Journal of Crystal Growth 270 (1) (2004) 232–249. doi:https://doi.org/10.1016/j.jcrysgro.2004.06.002.

[13] O. Weinstein, S. Brandon, Dynamics of partially faceted melt–crystal interfaces III: Three-dimensional computational approach and calculations, Journal of Crystal Growth 284 (1) (2005) 235–253. doi:https://doi.org/10.1016/j.jcrysgro.2005.06.031.

[14] C. Lan, C. Chen, Dynamic three-dimensional simulation of facet formation and segregation in Bridgman crystal growth, Journal of Crystal Growth 303 (1) (2007) 287–296. doi:https://doi.org/10.1016/j.jcrysgro.2006.11.333.

[15] A. Virozub, S. Brandon, Is it important to account for heat transport and interfacial attachment kinetics when calculating the shape of directionally solidified drops?, Journal of Crystal Growth 312 (16) (2010) 2472–2478. doi:https://doi.org/10.1016/j.jcrysgro.2010.05.025.

[16] O. Weinstein, W. Miller, Three-dimensional calculations of facets during Czochralski crystal growth, Journal of Crystal Growth 312 (7) (2010) 989–996. doi:https://doi.org/10.1016/j.jcrysgro.2009.12.071.

[17] A. Krauze, J. Virbulis, S. Zitzelsberger, G. Ratnieks, 3D modeling of growth ridge and edge facet formation in ¡100¿ floating zone silicon crystal growth process, Journal of Crystal Growth 520 (2019) 68–71. doi:https://doi.org/10.1016/j.jcrysgro.2019.04.030.

[18] A. Pirnia, B. T. Helenbrook, Analysis of faceted solidification in the hor-

izontal ribbon growth crystallization process, Journal of Crystal Growth 555 (2021) 125958. doi:10.1016/j.jcrysgro.2020.125958.

[19] A. Pirnia, B. T. Helenbrook, Physics of double faceted crystal growth in solidification processes, Journal of Crystal Growth 582 (2022) 126517. doi:10.1016/j.jcrysgro.2022.126517.

[20] J. A. Zoutendyk, Theoretical analysis of heat flow in horizontal ribbon growth from a melt, Journal of Applied Physics 49 (7) (1978) 3927–3932. doi:10.1063/1.325401.

[21] J. A. Zoutendyk, Analysis of forced convection heat flow effects in horizontal ribbon growth from the melt, Journal of Crystal Growth 50 (1) (1980) 83–93. doi:10.1016/0022-0248(80)90233-X.

[22] B. Kudo, Improvements in the horizontal ribbon growth technique for single crystal silicon, Journal of Crystal Growth 50 (1) (1980) 247–259. doi:10.1016/0022-0248(80)90248-1.

[23] P. D. Thomas, R. A. Brown, Rate limits in silicon sheet growth: The connections between vertical and horizontal methods, Journal of Crystal Growth 82 (1) (1987) 1–9. doi:10.1016/0022-0248(87)90157-6.

[24] P. Daggolu, A. Yeckel, C. E. Bleil, J. J. Derby, Thermal-capillary analysis of the horizontal ribbon growth of silicon crystals, Journal of Crystal Growth 355 (1) (2012) 129–139. doi:10.1016/j.jcrysgro.2012.06.055.

[25] P. Daggolu, A. Yeckel, C. E. Bleil, J. J. Derby, Stability limits for the horizontal ribbon growth of silicon crystals, Journal of Crystal Growth 363 (2013) 132–140. doi:10.1016/j.jcrysgro.2012.10.024.

[26] W. Miller, Some remarks on the undercooling of the Si(111) facet and the "Monte Carlo modeling of silicon crystal growth" by Kirk M. Beatty & Kenneth A. Jackson, J. Crystal Growth 211 (2000) 13, Journal of Crystal Growth 325 (1) (2011) 101–103. doi:https://doi.org/10.1016/j.jcrysgro.2011.03.031.

[27] K. A. Jackson, Response to: Some remarks on the undercooling of the si(1 1 1) facet and the "Monte Carlo modeling of silicon crystal growth" by Kirk M. Beatty & Kenneth A. Jackson, J. Crystal Growth 211 (2000), 13 by W. Miller, Journal of Crystal Growth 325 (1) (2011) 104. doi:https://doi.org/10.1016/j.jcrysgro.2011.03.040.

[28] N. Bagheri-Sadeghi, B. T. Helenbrook, Buoyancy and Marangoni effects on horizontal ribbon growth, Journal of Crystal Growth 596 (2022) 126822. doi:https://doi.org/10.1016/j.jcrysgro.2022.126822.

[29] K. A. Jackson, Kinetic Processes: Crystal Growth, Diffusion, and Phase Transitions in Materials, John Wiley & Sons, 2004. doi:https://doi.org/10.1002/3527603891.

[30] W. Obretenov, D. Kashchiev, V. Bostanov, Unified description of the rate of nucleation-mediated crystal growth, Journal of Crystal Growth 96 (4) (1989) 843–848. doi:https://doi.org/10.1016/0022-0248(89)90644-1.

[31] W. Hillig, A derivation of classical two-dimensional nucleation kinetics and the associated crystal growth laws, Acta Metallurgica 14 (12) (1966) 1868–1869. doi:https://doi.org/10.1016/0001-6160(66)90046-0.

[32] A. A. Chernov, Crystallization, Annual Review of Materials Science 3 (1) (1973) 397–454. doi:https://doi.org/10.1146/annurev.ms.03.080173.002145.

[33] D. Buta, M. Asta, J. J. Hoyt, Kinetic coefficient of steps at the Si(111) crystal-melt interface from molecular dynamics simulations, The Journal of Chemical Physics 127 (7) (2007) 074703. doi:https://doi.org/10.1063/1.2754682.

[34] B. Helenbrook, J. Hrdina, High-order adaptive arbitrary-Lagrangian–Eulerian (ALE) simulations of solidification, Computers & Fluids 167

(2018) 40–50. doi:https://doi.org/10.1016/j.compfluid.2018.02.028.

[35] T. Ciszek, Solid-liquid interface morphology of float-zoned silicon crystals, in: Semiconductor Silicon, Electrochemical Society New York, 1969, pp. 156–168.